




# Third-harmonic generation enhancement in an ITO nanoparticle-coated microresonator

STEVEN K. PAMPEL,<sup>1,\*</sup> KYUYOUNG BAE,<sup>2</sup> MO ZOHRABI,<sup>2</sup> MICHAEL GRAYSON,<sup>2</sup> THOMAS M. HORNING,<sup>1</sup> WOUNJHANG PARK,<sup>2,3</sup> AND JULIET T. GOPINATH<sup>1,2</sup> 

<sup>1</sup>Department of Physics, University of Boulder Colorado, Boulder, CO 80309, USA

<sup>2</sup>Department of Electrical, Computer, and Energy Engineering, University of Boulder Colorado, Boulder, CO 80309, USA

<sup>3</sup>Materials Science & Engineering Program, University of Colorado, Boulder, CO 80309, USA

\*[steven.pampel@colorado.edu](mailto:steven.pampel@colorado.edu)

**Abstract:** We report a ~3-fold enhancement of third-harmonic generation (THG) conversion efficiency using indium tin oxide (ITO) nanoparticles on the surface of an ultra-high- $Q$  silica microsphere. This is one of the largest microcavity-based THG enhancements reported. Phase-matching and spatial mode overlap are explored numerically to determine the microsphere radius (~29  $\mu\text{m}$ ) and resonant mode numbers that maximize THG. Furthermore, the ITO nanoparticles are uniformly bonded to the cavity surface by drop-casting, eliminating the need for complex fabrication. The significant improvement in THG conversion efficiency establishes functionalized ITO microcavities as a promising tool for broadband frequency conversion, nonlinear enhancement, and applications in integrated photonics.

© 2020 Optical Society of America under the terms of the [OSA Open Access Publishing Agreement](#)

## 1. Introduction

Whispering-gallery-mode (WGM) microresonators have garnered much interest due to their optical mode confinement and ability to effectuate strong nonlinear interactions on compact, low-power devices [1–5]. Applications in high-precision sensing [6,7], optical communications [8,9], and non-classical light generation [10,11] have all seen remarkable advancements as a result of the increased light-matter interaction length provided by microresonators. Many applications utilize third-order nonlinear effects such as four-wave mixing [12,13], stimulated Raman scattering [14,15], stimulated Brillouin scattering [16,17], and third-order sum frequency generation [18,19], which have all been studied in a wide variety of resonator geometries [20–23]. However, the efficiency of third-order nonlinear processes is severely constrained by the low  $\chi^{(3)}$  susceptibility in common optical materials, such as silica. Functionalized microcavities offer a novel solution to this problem, providing a way to substantially increase the Kerr nonlinearity ( $n_2$ ) of a resonator and thereby enable high-efficiency interactions [24–26].

Silica microspheres are particularly useful in the study of third-order nonlinear effects due to their ultra-high quality factors and relative ease of fabrication [27,28]. Silica is frequently used as a resonator material due to its favorable optical properties in the near-infrared region, i.e. ultra-low material absorption and inversion symmetry that prohibits the generation of competing  $\chi^{(2)}$  effects. Despite the many advantages of silica, its  $n_2$  is low ( $2.2\text{--}2.7 \times 10^{-20} \text{ m}^2/\text{W}$ ) [29,30], and is not sufficient for facilitating strong nonlinear effects at low pump powers [31]. Recent developments in functionalized microcavities provide a solution to this problem by exploiting the optical properties of highly nonlinear materials to substantially increase the  $n_2$  of a microresonator [24–26,32]. By coating the microresonator surface with highly nonlinear, functionalized organic molecules, high-efficiency nonlinear interactions can be realized while retaining the material benefits of silica [33]. Few molecules have been extensively studied for cavity functionalization, and uniform coating is typically achieved through relatively complex fabrication methods such as

chemical vapor deposition, spin-coating, or sputtering [24–26,32]. Due to the small diameter of the ITO nanoparticles (~9 nm), the application method of drop-casting can be used to achieve uniform surface-coating [34], avoiding the need for specialized fabrication equipment.

In this research, we use indium tin oxide (ITO) nanoparticles on the surface of an ultra-high- $Q$  silica microsphere to demonstrate a ~3-fold enhancement in third-harmonic generation. Bulk ITO has an exceptionally high  $n_2$  at its epsilon-near-zero wavelength (more than 10,000 times greater than the  $n_2$  of pure silica) [35]. Strong conductivity and optical transparency in the visible spectrum make ITO an attractive material for many applications [36], but large absorption near the Mie resonance has prevented bulk ITO from becoming a primary material in high- $Q$  microresonators. However, ITO nanoparticles have been shown to provide the desired nonlinearity of bulk ITO while minimizing the associated absorption loss [37]. Here, we achieve a microresonator that possesses both a high  $n_2$  and a high  $Q$ -factor for enhanced nonlinear effects.

## 2. Third-harmonic generation

Third-harmonic generation (THG) and third-order sum frequency generation (TSFG) occur when three pump photons annihilate to become one photon at a higher frequency. In the degenerate case (THG), each pump photon is of equal frequency, such that  $\omega_T = 3\omega_P$ , where  $\omega_T$  is the angular frequency of the generated photon and  $\omega_P$  is the angular frequency of the pump photon. In the non-degenerate case (TSFG), two of the three pump photons become Raman Stokes photons, such that  $\omega_T = \omega_P + \omega_{RS,1} + \omega_{RS,2}$ , where  $\omega_{RS,1}$  and  $\omega_{RS,2}$  are the Raman Stokes photons. Phase-matching conditions must be satisfied in order for THG or TSFG to occur. In a microcavity, phase-matching requires the effective index of the pump mode and THG mode to be equal. In order to fulfill this requirement, the dispersion profile of a WGM can be exploited to compensate for the effective index mismatch between the pump and THG modes. Due to the large difference between the pump and THG wavelengths, excitation of higher-order THG modes is necessary to match the effective indices.

Here, numerical simulations are performed using COMSOL Multiphysics [38] to determine the ideal silica microsphere radius that will satisfy phase-matching conditions and maximize spatial overlap between the pump and THG modes. A finite-difference eigenmode solver is used to find the effective indices corresponding to the pump (1550 nm) and THG (516.6 nm) eigenfrequencies of a pure silica sphere. Simulation results in Fig. 1 show the effective index of the resulting pump and THG modes as a function of microsphere radius. The intersection of the pump and higher-order THG modes indicate phase-matched radii that enable strong THG. A sphere radius range of 26  $\mu\text{m}$  to 35  $\mu\text{m}$  is chosen to provide a good balance between the quality factor and circulating power density in the cavity [39,40].

For efficient THG conversion in a microsphere, phase-matching of higher-order pump modes and THG modes is crucial. Thus, pump modes with a polar mode number  $l$  between 1 and 8 are examined to provide a range of possible interactions. For the phase-matched modes, spatial overlap is calculated to identify the microsphere radius that will generate the strongest THG [see Table 1]. The modal overlap factor is given by [41]:

$$\xi = \frac{\iint dr dz [E_{a,z}^*(r, z)]^3 E_{b,z}(r, z)}{\left[ \iint dr dz [E_{a,z}(r, z)^2] \right]^{\frac{3}{2}} \left[ \iint dr dz [E_{b,z}(r, z)^2] \right]^{\frac{1}{2}}}, \quad (1)$$

where  $E_{a(b),z}(r, z)$  is proportional to the  $z$ -component of the electric field distribution for the optical modes in the microsphere.

Spatial overlap depends on the distribution of the radial, polar, and azimuthal fields. Simulation results show mode overlap increasing proportionally to the polar mode number. The strongest overlap factor of ~0.3 occurs for the higher-order pump mode ( $l = 8$ ;  $n = 1$ ) and THG mode ( $l = 27$ ;  $n = 1$ ), corresponding to a sphere radius of 29.77  $\mu\text{m}$ . Mode profiles for phase-matched

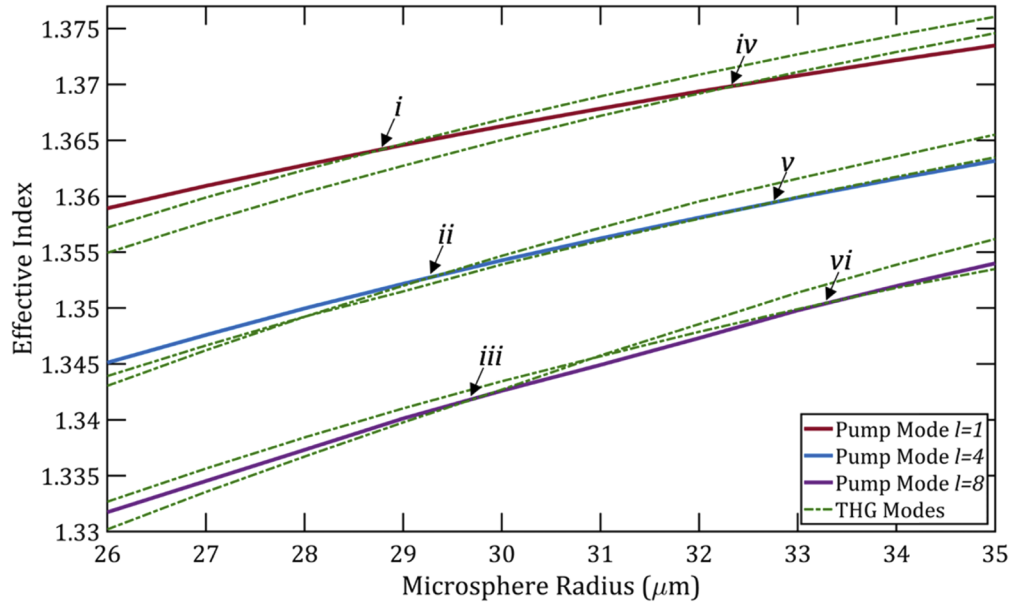


**Fig. 1.** Effective index as a function of radius for a pure silica microsphere. Fundamental ( $l=n=1$ ) and higher order ( $l=4, 8; 1 \leq n \leq 3$ ) TE pump modes at 1550 nm are tracked alongside higher-order THG modes ( $3 \leq l \leq 27; 1 \leq n \leq 3$ ) at 516.16 nm. Phase-matching between the pump modes and THG modes is achieved at intersection points *i-vi*.

modes *i* and *iii* are plotted in Figs. 2(a) and 2(b) respectively, showing  $|E_{a,z}|^2$  of the pump mode (left),  $|E_{b,z}|^2$  of the phase-matched THG mode (middle), and the overlap of the two modes (right). The overlap profile is calculated using  $E_{a,z}(r, z)^3 \times E_{b,z}(r, z)$ .

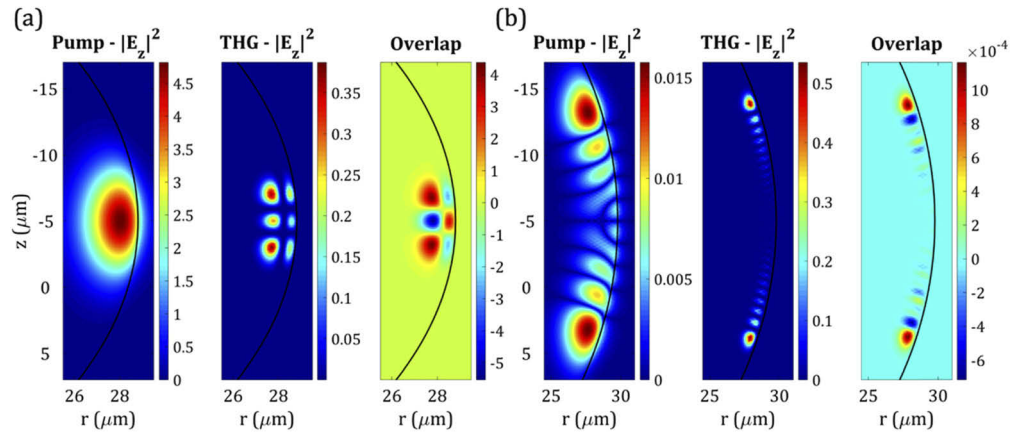


**Fig. 2.** (a) Overlap profile (right) for a phase-matched fundamental pump mode (left) and higher-order THG mode (middle) [point *i* - Fig. 1], corresponding to a radius of 28.81  $\mu\text{m}$  and mode overlap factor of 0.1543. (b) Overlap profile (right) for a phase-matched higher-order pump mode (left) and higher-order THG mode (middle) [point *iii* - Fig. 1], corresponding to a radius of 29.77  $\mu\text{m}$  and overlap factor of 0.3058. The overlap is calculated using  $E_{a,z}(r, z)^3 \times E_{b,z}(r, z)$ .

**Table 1. Mode overlap factor and radius for phase-matched modes**

	<i>i</i>	<i>ii</i>	<i>iii</i>	<i>iv</i>	<i>v</i>	<i>vi</i>
<b>R (μm)</b>	28.81	29.30	29.77	32.38	32.59	33.41
<b>ξ</b>	0.1543	0.2134	0.3058	0.1121	0.2091	0.1875

Based on the results of our phase-matching simulations, mode overlap calculations, and previous research on silica microspheres [19,24], a sphere radius of  $\sim 29\ \mu\text{m}$  is used in the experiment. Phase-matching conditions for the ITO-coated sphere are expected to be minimally impacted due to the small diameter of the nanoparticles and the small volume fraction of ITO/silica ( $\sim 10^{-8}$ ).

### 3. Experimental design

We use a continuously tunable diode laser (Toptica CTL 1550) followed by a polarization controller as a 1550 nm pump. The light is amplified using an erbium-doped fiber amplifier and launched into a tapered fiber. The field in the tapered fiber is evanescently coupled to the microsphere, with the output of the tapered fiber connected to an InGaAs photodetector (Newport 1811-FC). The resonator is mounted on a 3-axis translation stage (Thorlabs MAX313D) with 20 nm precision and imaged with a CCD camera [see Fig. 3(a)]. For coupling to the microsphere, we fabricate a silica tapered fiber, with a waist diameter of  $\sim 800\ \text{nm}$ , using motorized stages and a butane heat source. Mode-hop-free wavelength scanning is performed through piezo-actuation of the laser cavity and modulated by a triangle waveform. The silica microsphere is fabricated by applying arc discharges in a fiber fusion splicer to one end of a half-tapered fiber. The size of the sphere radius is controllable from  $20\ \mu\text{m}$  to  $100\ \mu\text{m}$ , determined by the initial size of the half-tapered fiber end and the number of arc discharges applied.

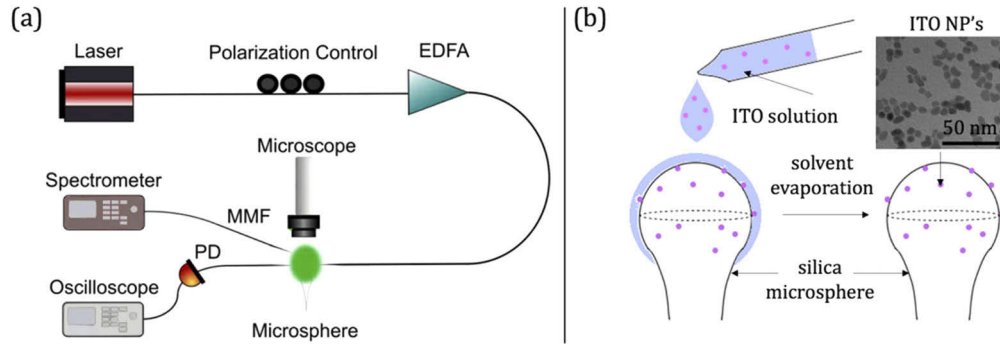


**Fig. 3.** (a) Experimental setup for the third-harmonic generation. A 1550 nm pump is generated by a continuous-wave laser, amplified, and launched into a tapered silica fiber. A  $60\ \mu\text{m}$  core fiber probe collects the scattered THG light from the microsphere surface. The transmission of the silica fiber is measured on an oscilloscope to ensure the desired coupling condition between the sphere and tapered fiber. (b) Diagram of drop-casting method used to coat the surface of the silica microsphere with ITO nanoparticles. A transmission electron micrograph image of ITO nanoparticles is shown in the upper right corner of (b). An average nanoparticle diameter of  $9.1 \pm 2.7\ \text{nm}$  is used to enhance nonlinearity and minimize absorption loss.

The ITO nanoparticles are synthesized to have an average diameter of  $9.1 \pm 2.7\ \text{nm}$  (measured using an electron micrograph image [see Fig. 3(b)]) to maximize nonlinear enhancement and minimize scattering loss. At this diameter, the Mie resonance of the particle is tuned to match

the measurement wavelength (1550 nm), providing maximum local electric field enhancement and increased nonlinearity. Larger nanoparticles ( $\sim 30$  nm diameter) were previously shown [37] to produce smaller enhancement and result in a lower  $Q$ -factor due to the increase in scattering loss. The nanoparticles are then diluted in a toluene colloidal solution to ensure the desired concentration on the sphere surface, and bonded to the silica sphere by method of drop-casting [see Fig. 3(b)]. The sphere is positioned upright during the application to avoid clumping of nanoparticles on the surface that can increase scattering and reduce the  $Q$ -factor. A single drop-coating of the solution is used to provide a good balance of nonlinear enhancement while retaining a high  $Q$ -factor. Additional coatings were previously shown [37] to provide a further increase in nonlinearity but resulted in substantially more absorption and a greatly reduced  $Q$ -factor.

#### 4. Results

THG power in the microresonator is collected with a 60-micron core multi-mode fiber positioned near the surface of the microsphere. The multi-mode fiber is connected to a spectrometer from which the THG spectra are acquired continuously at the rate of 1000/s with a laser scan rate of 50 Hz. For each input pump power, the resulting THG spectra are integrated and averaged to provide the final value of THG output power. As seen in Fig. 4, the ITO-coated sphere produces an average increase in THG power of  $186 \pm 24\%$ , with a maximum increase of 256% occurring at 5 mW of pump power. Cubic power dependence of the THG output is observed using pump powers from 2.5 mW to 7.5 mW [see Fig. 4(b)].

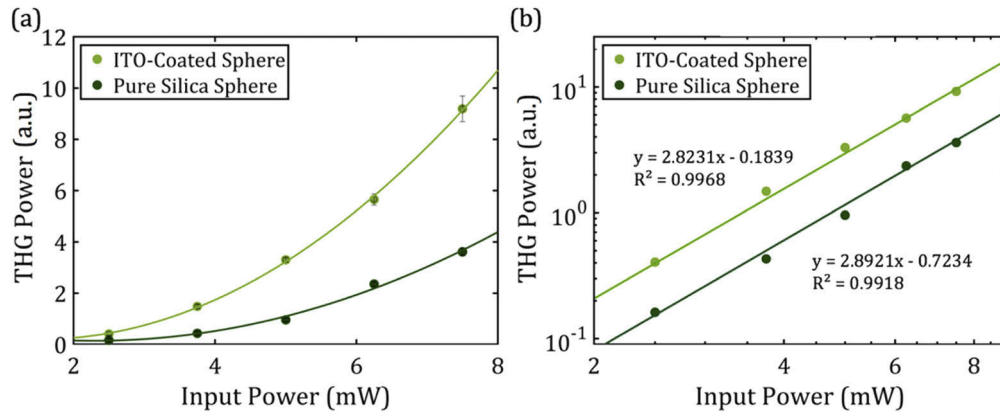


**Fig. 4.** (a) THG power as a function of pump power for a silica microsphere before and after application of ITO nanoparticles. The ITO-coated sphere shows an average increase of  $186 \pm 24\%$  over the pure silica sphere. (b) Log-log plot of THG power as a function of input pump power. Cubic dependence is observed for both the coated and uncoated sphere as indicated by the  $\sim 3$  coefficient for the slope of the linear fit.

The standard deviation of THG power is shown to increase proportionally to pump power as seen in the error bars of Fig. 4(a). This is likely due to increased thermo-optic effects at higher pump powers. In the presence of high intensity optical fields, large changes in temperature can induce a deviation in the circulating optical path which perturbs the resonance [42].

The power intensity of THG scales cubically in relation to pump power [18]. In Fig. 4(b), the 0.11 and 0.18 deviation from the theoretical slope coefficient of 3 is likely due to uncertainty in the lower bound of the power measurements which were slightly above the noise floor of the spectrometer. At pump powers greater than  $\sim 8$  mW, competing nonlinear effects such as Raman



scattering begin to dominate. When this occurs, energy in the pump photons is lost and the power relation between the pump input and THG output trends toward a linear dependence [19].

Optical microscope images of the pure silica sphere and ITO-coated microsphere are shown in Fig. 5(a). The images are captured at 5 mW of pump power, corresponding to a 256% increase in measured THG output. Spectrum measurements that correspond to the THG images in Fig. 5(a) are shown in Fig. 5(b), where THG power is measured at 519.05 nm. For a pump wavelength of 1554.45 nm, the theoretical THG wavelength is 518.15 nm, indicating an experimental variance of 0.17%. The deviation of 0.17% from the theoretical value is likely due to the optical resolution of the spectrometer and lack of calibration with respect to the laser.

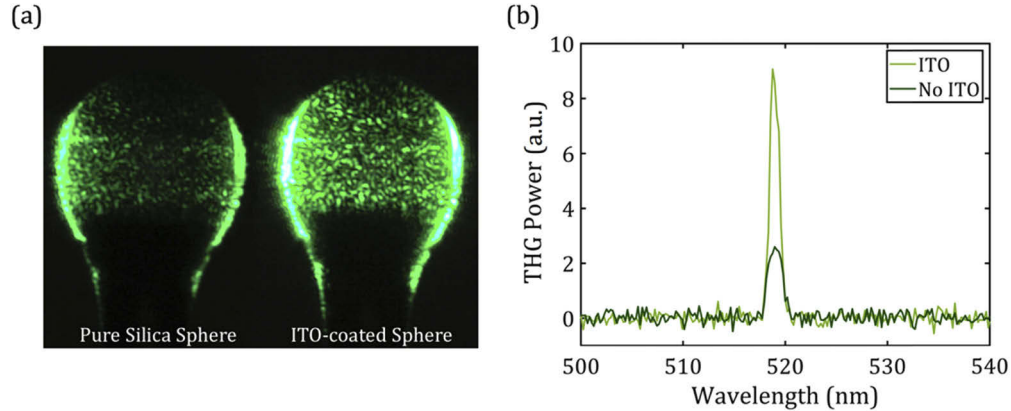


**Fig. 5.** (a) CCD images of THG light for the pure silica sphere and ITO-coated sphere, corresponding to a 256% increase in THG power. Images are captured at 5 mW of pump power. (b) THG power for the coated and uncoated spheres in Fig. 5(a). Relative THG power observed at 519.05 nm for a corresponding pump wavelength of 1554.45 nm, indicating a variance of 0.17% from theoretical THG value of 518.15 nm.

The same silica sphere is used for both coated and uncoated measurements, and coupling conditions are carefully replicated for each sphere with the aid of camera images and monitoring of the tapered fiber transmission spectrum. Both the pure silica sphere and coated sphere are critically coupled when THG data is collected. By tuning the wavelength at a given pump power, we are able to excite the same modes in the coated and uncoated spheres to ensure an accurate comparison. As pump power is increased, the pump wavelength is adjusted accordingly to counteract this thermally induced resonance shift, ensuring the double resonance condition of the pump and THG modes is maintained [24].

At higher pump powers, competing nonlinear effects such as stimulated Raman scattering (SRS), cascaded Raman scattering (CRS), and parametric oscillation can occur [40,43]. SRS occurs when the inelastic scattering of pump photons generates optical phonons, resulting in pump photons of lower energy. As an intrinsically phase-matched process, SRS often becomes the dominant effect in a microcavity when the threshold is exceeded. TSFG due to SRS and CRS in an ITO-coated sphere is shown in Figs. 6(a) and 6(b) respectively, where the summation of reduced energy photons and pump photons results visible emissions at wavelengths longer than the THG wavelength. For example, the spectrum in Fig. 6(a) is the result of one pump photon at 1549 nm and two Raman Stokes photons at 1667 nm summing to form one photon at 542 nm.

In a WGM microresonator, the efficiency of nonlinear processes is greatly impacted by the quality factor of the device. For THG, the converted power scales proportionally to  $(Q/V)^3$ , where  $Q$  is the quality factor and  $V$  is the optical mode volume [18]. Here,  $Q$ -factor data is extracted from the power transmission of the tapered fiber using the cavity ringdown method [44–46]. By fitting the decay envelope of the ringdown signal, we determine the decay constant  $\tau$  and use the

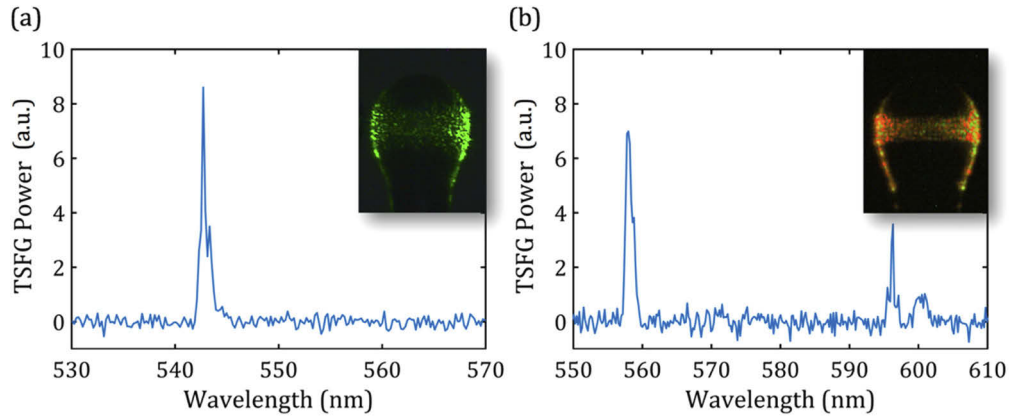


**Fig. 6.** (a) Spectral data measuring the power of TSFG due to SRS (input power of  $\sim 15$  mW) in an ITO-coated sphere. One pump photon at 1549 nm and two Raman Stokes photons at 1667 nm sum to form one photon at 542 nm ( $2/1667 + 1/1549 = 1/542$ ). (b) CRS-induced concomitant pump wavelengths sum to produce simultaneous visible emissions at 558 nm, 597 nm, and 601 nm (input power of  $\sim 20$  mW).

relation  $Q = \pi c \tau / \lambda$  to calculate the  $Q$ -factor. At  $\sim 20$   $\mu$ W of pump power, measurements are taken for both the pure and coated microspheres. Ringdown is measured when the microsphere is weakly coupled to the taper to reduce the presence of thermal effects. The pure silica sphere is determined to have a  $Q$ -factor of  $2.5 \times 10^8$  while the coated sphere has a  $Q$ -factor of  $3.6 \times 10^7$ , resulting in a reduction factor of 6.94 [see Fig. 7].

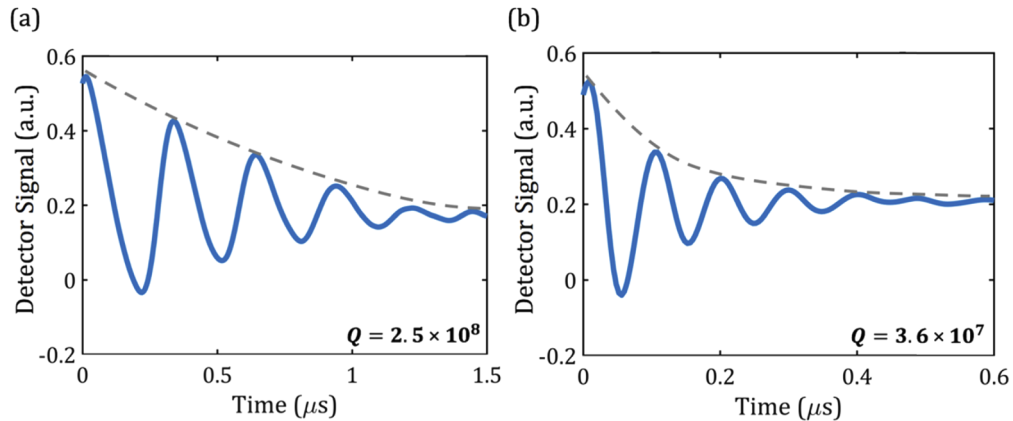


**Fig. 7.** (a) Cavity ringdown spectra (solid line) and decay envelope of pure silica sphere (dashed line).  $Q$ -factor is extracted by finding the decay constant and evaluating  $Q = \pi c \tau / \lambda$ . (b) Cavity ringdown spectra and decay envelope of the ITO-coated sphere. The quicker decay rate of the ITO-coated sphere can be seen in the curve of the decay envelope as well as the smaller time scale on the horizontal axis of the plot. The decrease in  $Q$ -factor is due to the increase in ITO-related absorption loss.

The relation between  $Q$ -factor and  $n_2$  plays an important role in determining the ideal volume fraction of ITO/silica to maximize nonlinear effects. An increase in nonlinearity can potentially be outweighed by the corresponding reduction in  $Q$ -factor as seen in the figure of merit ( $Q \times n_2$ ) comparisons in [37]. In this previous work, the  $n_2$  of a similarly sized ITO-coated and pure

silica sphere was shown to be  $7.2 \times 10^{-19} \text{ m}^2/\text{W}$  and  $1.8 \times 10^{-20} \text{ m}^2/\text{W}$  respectively, indicating that the ITO nanoparticles contribute  $7.02 \times 10^{-19} \text{ m}^2/\text{W}$  to the total  $n_2$  of the coated sphere. However, this 40-fold increase in  $n_2$  does not yield a similar increase in nonlinear effects as only a small fraction of the mode volume interacts with the nanoparticles on the surface of the sphere. Furthermore, this increase in  $n_2$  is offset by a 10-fold reduction in  $Q$ -factor due to increased absorption, resulting in an overall 3-fold increase in nonlinear effects. These results are in excellent agreement with the experimental results presented here.

$Q$ -factor measurements can be used in conjunction with the nonlinear coupling strength  $g$  to approximate THG conversion efficiency. When phase matching conditions are satisfied, the azimuthal mode numbers of the pump and THG modes  $m_a$  and  $m_b$  are related by  $3m_a \approx m_b$ , and the mode overlap factor  $\xi$  [see Table 1] can be used to approximate  $g$ . The mode overlap for the coated sphere is expected to be similar to that of the pure sphere given the small volume fraction of the ITO, so the maximum mode overlap factor of 0.3058 for a sphere radius of a  $29.77 \mu\text{m}$  is used here to evaluate  $g$ . In the case of critical coupling and zero detuning, nonlinear coupling strength is approximated by [41]:

$$g \approx \frac{\xi \sqrt{3} h \omega_a^2 \chi^{(3)}(r)}{\epsilon_0 4\pi R \sqrt{\epsilon_a^3 \epsilon_b}} \delta(3m_a - m_b), \quad (2)$$

where  $\omega_a$  is the angular frequency of the pump mode,  $R$  is the resonator radius, and  $\epsilon_{a(b)}$  is the relative permittivity of the sphere for the pump (visible) light. The third-order nonlinear susceptibility of the resonator must account for both the silica sphere and the ITO nanoparticles. Using the estimated effective  $n_2$  of  $7.2 \times 10^{-19} \text{ m}^2/\text{W}$ , we can estimate  $\chi^{(3)}$  using the relation  $\chi^{(3)} = (4/3)n_0^2 \epsilon_0 n_2$ . Assuming perfect phase matching, the THG conversion efficiency ( $\eta = P_P/P_{THG}^3$ ) of the resonator can then be expressed as [41]:

$$\eta = g^2 \frac{64\pi^2 Q_a^3 Q_b}{h\omega_a^6}, \quad (3)$$

where  $Q_{a(b)}$  are the quality factors for the fundamental pump mode and phase-matched higher-order THG mode. Using the experimentally determined  $Q$ -factor,  $Q_a = 3.6 \times 10^7$ , and approximating  $Q_b$  to be an order of magnitude smaller than  $Q_a$  [24,41], we arrive at an absolute conversion efficiency  $\eta' = P_P/P_{THG}^3$  of 0.0245 for a pump power of 2.5 mW. The uncoated silica sphere shows a conversion efficiency of  $\sim 1/3$  of the coated sphere ( $\eta' = 0.0097$ ), which is in strong agreement with experimental results. This value of  $\eta'$  is likely larger than what would be measured given the assumptions of  $g$  and  $\eta$ , and is only meant to provide a rough comparison to similar devices. A THG efficiency of 0.0256 is  $\sim 3$  orders of magnitude larger than a similar pure silica microsphere with  $Q_a = 1.0 \times 10^7$  [19], and compares favorably to other resonator geometries [24,47].

## 5. Conclusion

We have demonstrated a  $\sim 3$ -fold enhancement of third-harmonic generation (THG) conversion efficiency using indium tin oxide (ITO) nanoparticles on the surface of an ultra-high- $Q$  silica microsphere. The  $\sim 3$ -fold increase in nonlinear effects and  $\sim 7$ -fold decrease in the  $Q$ -factor of the microsphere was shown to be in excellent agreement with previous results for ITO-coated silica microspheres [37]. The cubic relation between THG and pump power was verified, and the effects of Raman-induced TSFG were explored. A numerical analysis of phase-matching and mode overlap was performed to identify the sphere radius ( $\sim 29 \mu\text{m}$ ) that maximizes THG for a pump wavelength of 1550 nm. To the best of the authors' knowledge, this is the first demonstration of THG enhancement using ITO nanoparticles, as well as one of the largest reported enhancements of THG in a silica microsphere [24–26,48–50]. We have also shown the benefits of ITO by



achieving uniform surface-coating through the drop-casting fabrication method. This work clearly demonstrates the nonlinear enhancement capabilities and fabrication advantages of ITO nanoparticles in microresonator-based applications. Although this research was limited to silica microspheres, ITO nanoparticles can be used for enhancement of any third-order nonlinear effects and applied to various resonator geometries.

## Funding

National Science Foundation (CCF 1838435); Office of Naval Research (N00014-19-1-2251, N00014-19-1-2382, N00014-19-1-2382 DURIP grant); Air Force Office of Scientific Research (FA9550-19-1-0364).

## Acknowledgements

The authors would like to acknowledge Dr. Jiangang Zhu and Dr. Hong Tang for technical discussions and guidance, and Dr. Igor Gamow and Dr. Elfriede Gamow for their support through the Gamow Scholarship, University of Colorado Boulder.

## Disclosures

The authors declare no conflicts of interest.

## References

1. G. C. Righini, Y. Dumeige, P. Féron, M. Ferrari, G. N. Conti, D. Ristic, and S. Soria, "Whispering gallery mode microresonators: Fundamentals and applications," *La Rivista del Nuovo Cimento* **34**, 435–488 (2011).
2. S. M. Spillane, T. J. Kippenberg, K. J. Vahala, K. W. Goh, E. Wilcut, and H. J. Kimble, "Ultra-high-Q toroidal microresonators for cavity quantum electrodynamics," *Phys. Rev. A* **71**(1), 013817 (2005).
3. T. Herr, V. Brasch, J. D. Jost, C. Y. Wang, N. M. Kondratiev, M. L. Gorodetsky, and T. J. Kippenberg, "Temporal solitons in optical microresonators," *Nat. Photonics* **8**(2), 145–152 (2014).
4. A. Chiasera, Y. Dumeige, P. Féron, M. Ferrari, Y. Jestin, G. Nunzi Conti, S. Pelli, S. Soria, and G. C. Righini, "Spherical whispering-gallery-mode microresonators," *Laser Photonics Rev.* **4**(3), 457–482 (2010).
5. T. J. Kippenberg, R. Holzwarth, and S. A. Diddams, "Microresonator-Based Optical Frequency Combs," *Science* **332**(6029), 555–559 (2011).
6. J. Zhu, S. K. Ozdemir, Y.-F. Xiao, L. Li, L. He, D.-R. Chen, and L. Yang, "On-chip single nanoparticle detection and sizing by mode splitting in an ultrahigh-Q microresonator," *Nat. Photonics* **4**(1), 46–49 (2010).
7. T. Reynolds, N. Riesen, A. Meldrum, X. Fan, J. M. M. Hall, T. M. Monro, and A. François, "Fluorescent and lasing whispering gallery mode microresonators for sensing applications: Fluorescent and lasing whispering gallery mode microresonators," *Laser Photonics Rev.* **11**(2), 1600265 (2017).
8. P. Marin-Palomo, J. N. Kemal, M. Karpov, A. Kordts, J. Pfeifle, M. H. P. Pfeiffer, P. Trocha, S. Wolf, V. Brasch, M. H. Anderson, R. Rosenberger, K. Vijayan, W. Freude, T. J. Kippenberg, and C. Koos, "Microresonator-based solitons for massively parallel coherent optical communications," *Nature* **546**(7657), 274–279 (2017).
9. J. Pfeifle, V. Brasch, M. Laueremann, Y. Yu, D. Wegner, T. Herr, K. Hartinger, P. Schindler, J. Li, D. Hillerkuss, R. Schmogrow, C. Weimann, R. Holzwarth, W. Freude, J. Leuthold, T. J. Kippenberg, and C. Koos, "Coherent terabit communications with microresonator Kerr frequency combs," *Nat. Photonics* **8**(5), 375–380 (2014).
10. S. Tanzilli, W. Tittel, M. Halder, O. Alibart, P. Baldi, N. Gisin, and H. Zbinden, "A photonic quantum information interface," *Nature* **437**(7055), 116–120 (2005).
11. P. Imany, J. A. Jaramillo-Villegas, O. D. Odele, K. Han, D. E. Leaird, J. M. Lukens, P. Lougovski, M. Qi, and A. M. Weiner, "50-GHz-spaced comb of high-dimensional frequency-bin entangled photons from an on-chip silicon nitride microresonator," *Opt. Express* **26**(2), 1825 (2018).
12. A. Fülöp, C. J. Krückel, D. Castelló-Lurbe, E. Silvestre, and V. Torres-Company, "Triply resonant coherent four-wave mixing in silicon nitride microresonators," *Opt. Lett.* **40**(17), 4006 (2015).
13. R. M. Camacho, "Entangled photon generation using four-wave mixing in azimuthally symmetric microresonators," *Opt. Express* **20**(20), 21977 (2012).
14. S. Blair and K. Zheng, "Microresonator-enhanced Raman amplification," *J. Opt. Soc. Am. B* **23**(6), 1117 (2006).
15. R.-S. Liu, W.-L. Jin, X.-C. Yu, Y.-C. Liu, and Y.-F. Xiao, "Enhanced Raman scattering of single nanoparticles in a high-Q whispering-gallery microresonator," *Phys. Rev. A* **91**(4), 043836 (2015).
16. B. Sturman and I. Breunig, "Brillouin lasing in whispering gallery micro-resonators," *New J. Phys.* **17**(12), 125006 (2015).
17. J. Li, M.-G. Suh, and K. Vahala, "Microresonator Brillouin gyroscope," *Optica* **4**(3), 346 (2017).

18. T. Carmon and K. J. Vahala, "Visible continuous emission from a silica microphotonic device by third-harmonic generation," *Nat. Phys.* **3**(6), 430–435 (2007).
19. D. Farnesi, A. Barucci, G. C. Righini, S. Berneschi, S. Soria, and G. Nunzi Conti, "Optical Frequency Conversion in Silica-Whispering-Gallery-Mode Microspherical Resonators," *Phys. Rev. Lett.* **112**(9), 093901 (2014).
20. G. Senthil Murugan, M. N. Petrovich, Y. Jung, J. S. Wilkinson, and M. N. Zervas, "Hollow-bottle optical microresonators," *Opt. Express* **19**(21), 20773 (2011).
21. D. K. Armani, T. J. Kippenberg, S. M. Spillane, and K. J. Vahala, "Ultra-high-Q toroid microcavity on a chip," *Nature* **421**(6926), 925–928 (2003).
22. D. D. Smith, H. Chang, and K. A. Fuller, "Whispering-gallery mode splitting in coupled microresonators," *J. Opt. Soc. Am. B* **20**(9), 1967 (2003).
23. M. Borselli, T. J. Johnson, and O. Painter, "Beyond the Rayleigh scattering limit in high-Q silicon microdisks: theory and experiment," *Opt. Express* **13**(5), 1515 (2005).
24. J. Chen, X. Shen, S.-J. Tang, Q.-T. Cao, Q. Gong, and Y.-F. Xiao, "Microcavity Nonlinear Optics with an Organically Functionalized Surface," *Phys. Rev. Lett.* **123**(17), 173902 (2019).
25. X. Shen, R. C. Beltran, V. Diep, S. Soltani, and A. M. Armani, "Organically modified microresonators for high efficiency microlasers," in *Frontiers in Optics 2017* (OSA, 2017), p. FTh3A.2.
26. M. Wang, X. Jin, F. Li, and K. Wang, "Analysis and application of whispering gallery modes of the triple-layer-coated microsphere resonator," *MATEC Web Conf.* **189**, 01009 (2018).
27. G. Frigenti, D. Farnesi, G. Nunzi Conti, and S. Soria, "Nonlinear Optics in Microspherical Resonators," *Micromachines* **11**(3), 303 (2020).
28. J. C. Knight, G. Cheung, F. Jacques, and T. A. Birks, "Phase-matched excitation of whispering-gallery-mode resonances by a fiber taper," *Opt. Lett.* **22**(15), 1129 (1997).
29. D. Milam, "Review and assessment of measured values of the nonlinear refractive-index coefficient of fused silica," *Appl. Opt.* **37**(3), 546 (1998).
30. K. S. Kim, W. A. Reed, K. W. Quoi, and R. H. Stolen, "Measurement of the nonlinear index of silica-core and dispersion-shifted fibers," *Opt. Lett.* **19**(4), 257 (1994).
31. U. Gubler and C. Bosshard, "Optical third-harmonic generation of fused silica in gas atmosphere: Absolute value of the third-order nonlinear optical susceptibility  $\chi$  (3)," *Phys. Rev. B* **61**(16), 10702–10710 (2000).
32. J. L. Dominguez-Juarez, G. Kozyreff, and J. Martorell, "Whispering gallery microresonators for second harmonic light generation from a low number of small molecules," *Nat. Commun.* **2**(1), 254 (2011).
33. T. M. Benson, S. V. Boriskina, P. Sewell, A. Vukovic, S. C. Greedy, and A. I. Nosich, "MICRO-OPTICAL RESONATORS FOR MICROLASERS AND INTEGRATED OPTOELECTRONICS," in *Frontiers in Planar Lightwave Circuit Technology*, S. Janz, J. Ctyroky, and S. Tanev, eds., NATO Science Series II: Mathematics, Physics and Chemistry (Kluwer Academic Publishers, 2006), Vol. 216, pp. 39–70.
34. A. A. M. Farag and I. S. Yahia, "Structural, absorption and optical dispersion characteristics of rhodamine B thin films prepared by drop casting technique," *Opt. Commun.* **283**(21), 4310–4317 (2010).
35. M. Z. Alam, I. De Leon, and R. W. Boyd, "Large optical nonlinearity of indium tin oxide in its epsilon-near-zero region," *Science* **352**(6287), 795–797 (2016).
36. N. Kometani and M. Fujii, "Solvochemical Synthesis of ITO Nanoparticles and Their Application to the Transparent Conductive Film," *The Review of High Pressure Science and Technology* **22**(2), 129–134 (2012).
37. K. Bae, J. Zhu, M. B. Grayson, M. Zohrabi, C. Wolenski, T. M. Horning, J. T. Gopinath, and W. Park, "High-quality factor, nonlinear indium tin oxide nanoparticle-coated silica microsphere," in *Nonlinear Optics (NLO)* (OSA, 2019), p. NTu3B.6.
38. *COMSOL Multiphysics, Version 5.0*, COMSOL, Inc., (n.d.).
39. M. L. Gorodetsky, A. D. Pryamikov, and V. S. Ilchenko, "Rayleigh scattering in high-Q microspheres," *J. Opt. Soc. Am. B* **17**(6), 1051 (2000).
40. S. M. Spillane, T. J. Kippenberg, and K. J. Vahala, "Ultralow-threshold Raman laser using a spherical dielectric microcavity," *Nature* **415**(6872), 621–623 (2002).
41. J. B. Surya, X. Guo, C.-L. Zou, and H. X. Tang, "Efficient third-harmonic generation in composite aluminum nitride/silicon nitride microrings," *Optica* **5**(2), 103 (2018).
42. T. Carmon, L. Yang, and K. J. Vahala, "Dynamical thermal behavior and thermal self-stability of microcavities," *Opt. Express* **12**(20), 4742 (2004).
43. T. J. Kippenberg, S. M. Spillane, and K. J. Vahala, "Kerr-Nonlinearity Optical Parametric Oscillation in an Ultrahigh-Q Toroid Microcavity," *Phys. Rev. Lett.* **93**(8), 083904 (2004).
44. I. S. Grudinin, V. S. Ilchenko, and L. Maleki, "Ultrahigh optical Q factors of crystalline resonators in the linear regime," *Phys. Rev. A* **74**(6), 063806 (2006).
45. Y. Dumeige, S. Trebaol, L. Ghiša, T. K. N. Nguyễn, H. Tavernier, and P. Féron, "Determination of coupling regime of high-Q resonators and optical gain of highly selective amplifiers," *J. Opt. Soc. Am. B* **25**(12), 2073 (2008).
46. M. Pöllinger, D. O'Shea, F. Warken, and A. Rauschenbeutel, "Ultrahigh-Q Tunable Whispering-Gallery-Mode Microresonator," *Phys. Rev. Lett.* **103**(5), 053901 (2009).
47. Y. Li, S. H. Wang, Y. Tian, W. L. Ho, Y. Li, L. Wang, R. R. Davidson, B. E. Little, and S. T. Chu, "Third-harmonic generation in CMOS-compatible highly doped silica micro-ring resonator," *Opt. Express* **28**(1), 641 (2020).

48. J. Bravo-Abad, A. Rodríguez, P. Bermel, S. G. Johnson, J. D. Joannopoulos, and M. Soljacic, "Enhanced nonlinear optics in photonic-crystal microcavities," *Opt. Express* **15**(24), 16161 (2007).
49. M. Clementi, K. Debnath, M. Sotto, A. Barone, A. Z. Khokhar, T. D. Bucio, S. Saito, F. Y. Gardes, D. Bajoni, and M. Galli, "Cavity-enhanced harmonic generation in silicon rich nitride photonic crystal microresonators," *Appl. Phys. Lett.* **114**(13), 131103 (2019).
50. J. B. Lassiter, X. Chen, X. Liu, C. Ciraci, T. B. Hoang, S. Larouche, S.-H. Oh, M. H. Mikkelsen, and D. R. Smith, "Third-Harmonic Generation Enhancement by Film-Coupled Plasmonic Stripe Resonators," *ACS Photonics* **1**(11), 1212–1217 (2014).